Discontinuous-Current Mode Operation of a Two-Phase Interleaved Boost DC–DC Converter With Coupled Inductor

Fei Yang, *Member, IEEE*, Xinbo Ruan, *Fellow, IEEE*, Gang Wu, *Student Member, IEEE*, and Zhihong Ye, *Member, IEEE*

***Abstract*—A two-phase interleaved boost dc–dc converter with an inversely coupled inductor in a discontinuous-current mode (DCM) is analyzed by the equivalent inductance method. Coupling effects on the circuit statuses are described, and a forced conduction of the power diode or reverse-paralleled diode of MOSFET is caused by coupling. As a result, three major circuit statuses are figured out according to the physical relationship between the input–output voltage ratio and the coupling coefficient, and their condition boundaries are used to classify the DCM operation modes. Then, considering the load (duty cycle) variation, ten DCM operation modes are comprehensively analyzed. The analysis can be used to make an easy prediction of operation modes, and extended to the analysis of an interleaved buck converter or buck/boost bidirectional converter with a coupled inductor in DCM. At last, a 300-W prototype is built and tested in the lab to verify the analysis.**

***Index Terms*—Coupling circuits, dc–dc power conversion, discontinuous-current mode (DCM), interleaved boost converter.**

I. Introduction

THE interleaved boost converter with an inversely coupled inductor is widely used as an interface converter in applications that require a high power density and high efficiency, such as electrical vehicles and hybrid electrical vehicles [1]–[4], fuel cell vehicles [5], photovoltaic (PV) power systems [6], and power factor correction [7], [8]. In dc–dc applications, the coupled inductor is often designed to be closely coupled for a high efficiency under a heavy load, and the inductor winding current normally operates in continuous-current mode (CCM) [9]–[12]. However, in some applications, like the vehicle power system or PV power system, the converter may work under a relatively light-load condition for a period of time or may have a wide range of loads. In that case, the inductor winding current flows in a discontinuous-current mode (DCM). For the research and converter design, the characteristics of a converter in DCM are also of significance.

Due to the discontinuous current in each winding and mutual effects caused by the coupled inductor in multiple phases, DCM produces more circuit statuses in one switching cycle than CCM, and it means more operation modes under different conditions. Some publications have examined behaviors and operation modes of the multiphase interleaved boost converter with a coupled inductor in DCM [13]–[16]. Huang *et al.* [13] focus on the current ringing of a multiphase interleaved boost dc–dc converter in DCM and has a limited analysis of its operation modes. Ray *et al.* [14] analyze some key dc performances of an interleaved boost dc–dc converter with a coupled inductor in three DCM and two CCM operation modes, separately, including dc voltage gain, input current ripple, inductor current ripple, and output voltage ripple. Barry *et al.* [15] provide a more comprehensive analysis of DCM operation modes for a two-phase interleaved boost converter with a discrete or coupled inductor, of which ten DCM operation modes and their boundary conditions are analyzed. However, the operation modes are presented directly with a flowchart, and one possible operation mode occurred under a relatively weak coupling condition (Mode 5 as shown in this paper) is missing. Wu *et al.* [16] analyze the operation modes of dual-interleaved buck and boost converters with an interphase transformer, and presents eight converter subcircuits and seven DCM major operation regions according to the relationship of the voltage ratio against to the duty cycle. However, the operation modes are classified according to circuit analysis and simulations, and their relationship are rarely explained. Although available researches have presented a mass of operation modes and their boundary conditions, the physical reasons why a converter has those modes and what kind of relationship those modes have are not described clearly enough. Moreover, most analysis is based on a strong coupled inductor, so some operation modes under a relatively weak coupling condition may be missed.

This paper analyzed the DCM operation modes of a two-phase interleaved boost dc–dc converter with a coupled inductor. First, based on a qualitative and quantitative analysis of the equivalent

Manuscript received August 21, 2016; revised December 25, 2016; accepted February 3, 2017. Date of publication February 15, 2017; date of current version October 6, 2017. This work was supported by Lite-On Technology, Corp., and Natural Science Foundation of Jiangsu Province No. BK20160837. Recommended for publication by Associate Editor K.-H. Chen. Recommended for publication by Associate Editor K.-H. Chen.

F. Yang is with the School of Automation, Nanjing University of Science and Technology, Nanjing 210016, China (e-mail: yangfei@njust.edu.cn).

X. Ruan and G. Wu are with the Center for More-Electric-Aircraft Power System, College of Automation Engineering, Nanjing University of Aeronautics and Astronautics, Nanjing 210016, China (e-mail: ruanxb@nuaa.edu.cn; wugang@nuaa.edu.cn).

Z. Ye is with Lite-On Technology Power SBG ATD-NJ R&D Center, Nanjing 210019, China (e-mail: Sam.Ye@liteon.com).

Color versions of one or more of the figures in this paper are available online at http://ieeexplore.ieee.org.

Digital Object Identifier 10.1109/TPEL.2017.2669401

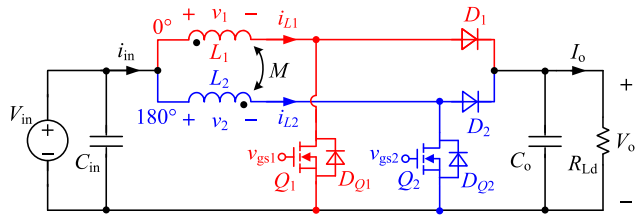

Fig. 1. Two-phase interleaved boost dc–dc converter with a coupled inductor.

inductance of the winding current, the circuit statuses are classified into three major conditions, which just depend on the physical relations of the coupling coefficient and the input–output voltage ratio. Then, ten DCM operation modes are described in detail considering the variation of load (duty cycle), which structure all the possible operation modes in a map. The corresponding boundary of each operation mode is presented for the prediction of the converter operation. The analysis and classification can also be extended to an interleaved buck converter or buck/boost bidirectional converter with a coupled inductor in DCM. Section II analyzed the coupling effects on the circuit statuses. Section III described the operation modes and their boundaries. Section IV gave experimental verifications with a 300-W prototype using two coupled inductors in a weak and strong coupling, separately.

II. Interleaved Boost DC–DC Converter in DCM With a Coupled Inductor

A. Coupled Inductor and Equivalent Inductance

Fig. 1 shows a two-phase interleaved boost dc–dc converter with an inversely coupled inductor, where $V_{\rm in}$ is the input voltage, V_o is the output voltage, v_1 and v_2 are the voltages applied on Winding 1 and Winding 2, i_{L1} and i_{L2} are the inductor winding currents, L_1 and L_2 are the self-inductance of the two windings, and M is the mutual-inductance, Q_1 and Q_2 are the power MOSFET with reverse-paralleled diodes D_{Q1} and D_{Q2}, and D_1 and D_2 are the power diodes.

Assuming that the two windings of the coupled inductor are identical, i.e., $L_1 = L_2 = L_{cp}$, and the coupling coefficient $\alpha = M/L_{cp}$. The circuit equation for the coupled inductor is

$$\begin{cases} v_1 = L_{cp}\dfrac{di_{L1}}{dt} - M\dfrac{di_{L2}}{dt} = L_{cp}\dfrac{di_{L1}}{dt} - \alpha L_{cp}\dfrac{di_{L2}}{dt} \\ v_2 = L_{cp}\dfrac{di_{L2}}{dt} - M\dfrac{di_{L1}}{dt} = L_{cp}\dfrac{di_{L2}}{dt} - \alpha L_{cp}\dfrac{di_{L1}}{dt} \end{cases}. \quad (1)$$

On the analysis of a coupled inductor, although the three-inductor model or the transformer and inductor model is simple and easy to understand [17]–[19], in order to obtain the inductor winding current waveforms directly, we use the equivalent inductance method in this paper. First, an equivalent inductance $L_{\rm eq}$ is defined as [20]:

$$v_j = L_{\rm eq}\frac{di_{L\rm j}}{dt}, \quad (j = 1, 2) \quad (2)$$

where v_j is the voltage applied on Winding j, and i_{Lj} represents the current flowing through Winding j.

When one inductor winding current keeps 0 ($di_{Lj}/dt = 0$), $L_{\rm eq}$ for the other winding current is L_{cp} from (1), and vice versa.

When currents flow through both windings ($di_{Lj}/dt \neq 0$), (1) can be rewritten as

$$\begin{cases} v_1 + \alpha v_2 = \left(1-\alpha^2\right) L_{cp} \cdot \dfrac{di_{L1}}{dt} \\ v_2 + \alpha v_1 = \left(1-\alpha^2\right) L_{cp} \cdot \dfrac{di_{L2}}{dt} \end{cases}$$

$$\Rightarrow \begin{cases} v_1 = \dfrac{\left(1-\alpha^2\right) L_{cp}}{1+\alpha\left(v_2/v_1\right)} \cdot \dfrac{di_{L1}}{dt} \\ v_2 = \dfrac{\left(1-\alpha^2\right) L_{cp}}{1+\alpha\left(v_1/v_2\right)} \cdot \dfrac{di_{L2}}{dt} \end{cases} \quad (3)$$

and the expressions of $L_{\rm eq}$ can be derived when v_1 and v_2 are known. Normally v_1 (v_2) equals $V_{\rm in}$ when Q_1 or D_{Q1} (Q_2 or D_{Q2}) conducts, and equals ($V_{\rm in} - V_o$) when $Q_1(Q_2)$ turns OFF and $D_1(D_2)$ conducts. For example, when Q_1 is ON and Q_2 is OFF, $v_1 = V_{\rm in}$ and $v_2 = V_{\rm in} - V_o$. From (3), the equivalent inductance of Winding 1 and Winding 2 is $L_{\rm eq1} = [(V_{\rm in}/V_o)(1-\alpha^2)L_{cp}]/[(1+\alpha)(V_{\rm in}/V_o) - \alpha]$ and $L_{\rm eq3} = [(1 - V_{\rm in}/V_o)(1-\alpha^2)L_{cp}]/[1-(1+\alpha)(V_{\rm in}/V_o)]$ respectively [8].

In summary, the expressions of $L_{\rm eq}$ for the two windings under different switch conditions are derived and shown in Table I. When α and L_{cp} are fixed, $L_{\rm eq2}$ is constant and always positive, and $L_{\rm eq1}$ and $L_{\rm eq3}$ have a relation with $V_{\rm in}/V_o$ and α. It should be noted that $L_{\rm eq}$, which impacts the current slope, is just used to calculate the inductor current waveform, so its value is only of significance in mathematics and may be positive, negative, or infinite.

If the quantitative relationship between $L_{\rm eq}$, $V_{\rm in}/V_o$, and α can be figured out, all the possible DCM current waveforms and operation modes for the converter in Fig. 1 can be obtained.

For $L_{\rm eq1}$, its numerator is always positive, and its denominator equals 0 when the coupling-coefficient satisfies

$$\alpha_{b1} = V_{\rm in}/(V_o - V_{\rm in}) = (V_{\rm in}/V_o)/[1-(V_{\rm in}/V_o)]. \quad (4a)$$

When the designed $\alpha < \alpha_{b1}$, $V_{\rm in}/V_o > \alpha/(1+\alpha)$, and $L_{\rm eq1} > 0$; when $\alpha = \alpha_{b1}$, $V_{\rm in}/V_o = \alpha/(1+\alpha)$, and $L_{\rm eq1}$ is infinite; when $\alpha > \alpha_{b1}$, $V_{\rm in}/V_o < \alpha/(1+\alpha)$, and $L_{\rm eq1} < 0$. α_{b1} increases as $V_{\rm in}/V_o$ increases. For $\alpha \leq 1$: when $V_{\rm in}/V_o < 0.5$, $\alpha_{b1} < 1$, and $L_{\rm eq1}$ is positive or negative depending on the relation between $V_{\rm in}/V_o$ and α; when $V_{\rm in}/V_o \geq 0.5$, $\alpha_{b1} \geq 1$, and $L_{\rm eq1}$ keeps a positive value.

For $L_{\rm eq3}$, its numerator is always positive and its denominator equals 0 when

$$\alpha_{b2} = (V_o - V_{\rm in})/V_{\rm in} = [1-(V_{\rm in}/V_o)]/(V_{\rm in}/V_o). \quad (4b)$$

When $\alpha < \alpha_{b2}$, $V_{\rm in}/V_o < 1/(1+\alpha)$, and $L_{\rm eq3} > 0$; when $\alpha = \alpha_{b2}$, $V_{\rm in}/V_o = 1/(1+\alpha)$, and $L_{\rm eq1}$ is infinite; when $\alpha > \alpha_{b2}$, $V_{\rm in}/V_o > 1/(1+\alpha)$, and $L_{\rm eq1} < 0$. α_{b2} decreases as $V_{\rm in}/V_o$ increases. For $\alpha < 1$: when $V_{\rm in}/V_o < 0.5$, $\alpha_{b2} > 1 > \alpha$, and $L_{\rm eq3}$ is always a positive value; when $V_{\rm in}/V_o \geq 0.5$, $\alpha_{b2} \leq 1$, and $L_{\rm eq3}$ is positive or negative depending on the relationship between $V_{\rm in}/V_o$ and α.

TABLE I
EQUIVALENT INDUCTANCES OF TWO WINDINGS

	Q_1 is ON, and Q_2 is OFF ($v_1 = V_{\rm in}$, $v_2 = V_{\rm in} - V_o$)	Q_1 and Q_2 are both ON or OFF ($v_1 = v_2 = V_{\rm in}$ or $v_1 = v_2 = V_{\rm in} - V_o$)	Q_1 is OFF, and Q_2 is ON ($v_1 = V_{\rm in} - V_o$, $v_2 = V_{\rm in}$)	$di_{L1}/dt = 0$ ($i_{L1} = 0$) or $di_{L2}/dt = 0$ ($i_{L2} = 0$)
Winding 1	$L_{eq1} = \frac{(V_{\rm in}/V_o)(1-\alpha^2)}{(1+\alpha)(V_{\rm in}/V_o)-\alpha} L_{cp}$	$L_{eq2} = (1-\alpha)L_{cp}$	$L_{eq3} = \frac{(1-V_{\rm in}/V_o)(1-\alpha^2)}{1-(1+\alpha)(V_{\rm in}/V_o)} L_{cp}$	L_{cp}
Winding 2	$L_{eq3} = \frac{(1-V_{\rm in}/V_o)(1-\alpha^2)}{1-(1+\alpha)(V_{\rm in}/V_o)} L_{cp}$	$L_{eq2} = (1-\alpha)L_{cp}$	$L_{eq1} = \frac{(V_{\rm in}/V_o)(1-\alpha^2)}{(1+\alpha)(V_{\rm in}/V_o)-\alpha} L_{cp}$	L_{cp}

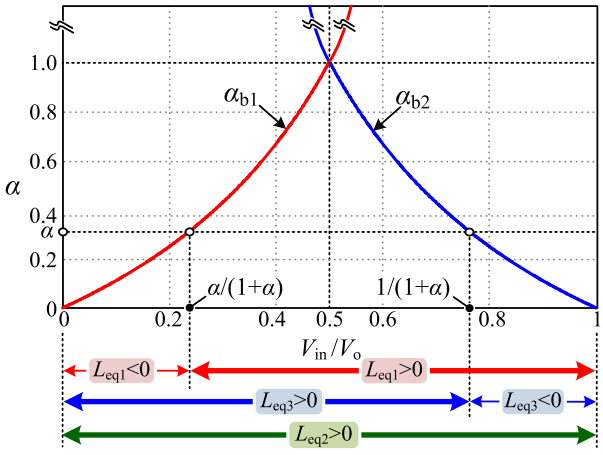

Fig. 2. α_{b1} and α_{b2} as functions of $V_{\rm in}/V_o$ and sign distributions of $L_{\rm eq1}$, $L_{\rm eq2}$, and $L_{\rm eq3}$.

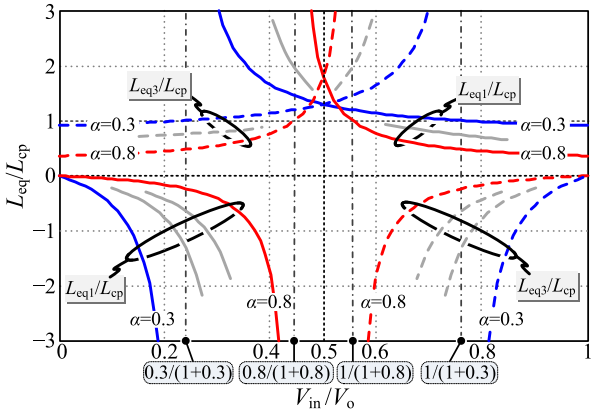

Fig. 3. $L_{\rm eq1}/L_{cp}$ and $L_{\rm eq3}/L_{cp}$ varied with $V_{\rm in}/V_o$ at different α.

α_{b1} and α_{b2} are calculated as functions of $V_{\rm in}/V_o$, as shown in Fig. 2. In summary, for a designed coupling-coefficient α: when $V_{\rm in}/V_o < \alpha/(1+\alpha)$, i.e., $\alpha > \alpha_{b1}$, $L_{\rm eq1} < 0$, $L_{\rm eq2} > 0$, and $L_{\rm eq3} > 0$; when $\alpha/(1+\alpha) < V_{\rm in}/V_o < 1/(1+\alpha)$, i.e., $\alpha < \alpha_{b1}$ and $\alpha < \alpha_{b2}$, $L_{\rm eq1} > 0$, $L_{\rm eq2} > 0$ and $L_{\rm eq3} > 0$; when $V_{\rm in}/V_o > 1/(1+\alpha)$, i.e., $\alpha > \alpha_{b2}$, $L_{\rm eq1} > 0$, $L_{\rm eq2} > 0$, and $L_{\rm eq3} < 0$.

For a quantitative variation of $L_{\rm eq}$, Fig. 3 depicts $L_{\rm eq1}/L_{cp}$ (solid line) and $L_{\rm eq3}/L_{cp}$ (dash line), both of which are varied with $V_{\rm in}/V_o$ at different coupling coefficients. Here, we take $\alpha = 0.3$ and $\alpha = 0.8$ as examples. For a fixed α, $L_{\rm eq1}$ and $L_{\rm eq3}$ are symmetric at $V_{\rm in}/V_o = 0.5$: when $V_{\rm in}/V_o < \alpha/(1+\alpha)$, $L_{\rm eq1} < 0$, and $L_{\rm eq1}$ decreases from 0 to infinite as $V_{\rm in}/V_o$ increases; when $V_{\rm in}/V_o > \alpha/(1+\alpha)$, $L_{\rm eq1} > 0$, and $L_{\rm eq1}$ decreases from infinite to a positive value as $V_{\rm in}/V_o$ increases. While when $V_{\rm in}/V_o < 1/(1+\alpha)$, $L_{\rm eq3} > 0$, and $L_{\rm eq3}$ increases from a positive value to infinite as $V_{\rm in}/V_o$ increases; when $V_{\rm in}/V_o > 1/(1+\alpha)$, $L_{\rm eq3} < 0$, and $|L_{\rm eq3}|$ decreases from infinite to 0 as $V_{\rm in}/V_o$ increases.

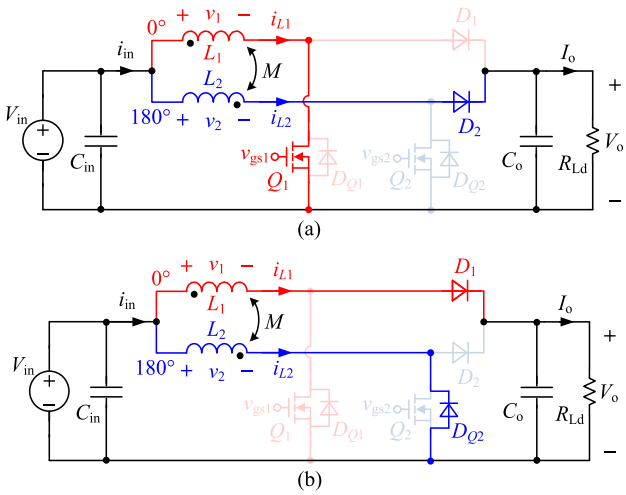

Fig. 4. Coupling effects on circuit statuses (a) for $V_{\rm in}/V_o > 1/(1+\alpha)$, turn-on of Q_1 leads to conduction of D_2, and (b) for $V_{\rm in}/V_o < \alpha/(1+\alpha)$, turn-off of Q_1 leads to conduction of D_{Q2}.

B. Coupling Effects on Circuit Operational Statuses

From Fig. 1, the turn-on and turn-off of Q_1 will change the voltage applied on Winding 1 v_1, as well as v_2, which lead to the modification of voltages applied on Q_2 and D_2. Similarly, the switch-status transformation of Q_2 also changes the voltage applied on Q_1 and D_1. Take Phase 1 as an example:

1) The winding currents of two phases have reached 0 initially, when Q_1 turns ON, $v_1 = V_{\rm in}$ and $v_2 = -\alpha V_{\rm in}$. Therfore, the voltage applied on the drain source of Q_2, $v_{ds\_Q2} = V_{\rm in} - v_2 = (1+\alpha)V_{\rm in} > 0$, and the reverse-paralleled diode of Q_2, D_{Q2} will not conduct. Simultaneously, the voltage applied on D_2, $v_{D2} = V_{\rm in} - v_2 - V_o = (1+\alpha)V_{\rm in} - V_o$. If $V_{\rm in}/V_o < 1/(1+\alpha)$, $v_{D2} \le 0$ and the current of Winding 2 remains 0. Otherwise, if $V_{\rm in}/V_o > 1/(1+\alpha)$, $v_{D2} > 0$ and D_2 will conduct immediatelly (assuming that the forward-bias voltage of D_2 is 0) and a positive direction current flows through Winding 2, as shown in Fig. 4(a).

TABLE II
COUPLING EFFECTS ON THE CIRCUIT STATUSES OF PHASE 1

	$V_{\rm in}/V_o < \alpha/(1+\alpha)$	$\alpha/(1+\alpha) \le V_{\rm in}/V_o \le 1/(1+\alpha)$	$V_{\rm in}/V_o > 1/(1+\alpha)$
Q_1 turns ON	D_2 does not conduct	D_2 does not conduct D_{Q2} does not conduct	D_2 conducts and i_{L2} flows in the positive direction (see Fig. 4(a))
Q_1 turns OFF	D_{Q2} conducts and i_{L2} flows in the negative direction (see Fig. 4(b))	D_2 does not conduct D_{Q2} does not conduct	D_{Q2} does not conduct

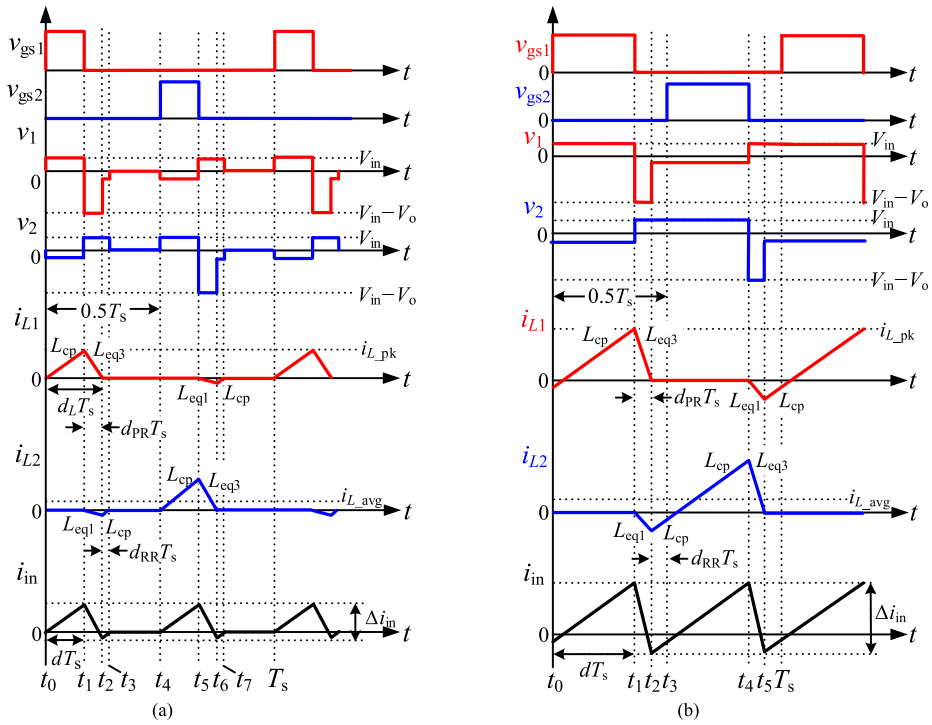

Fig. 5. Waveforms of (a) Mode 1a and (b) Mode 1b in a switching cycle when $d \le 0.5$ and $V_{\rm in}/V_o < \alpha/(1+\alpha)$.

2) For $V_{\rm in}/V_o < 1/(1+\alpha)$, assuming that the current of Winding 2 keeps 0 during the conduction period of Q_1, when Q_1 turns off, $v_1 = V_{\rm in} - V_o$ and $v_2 = -\alpha(V_{\rm in} - V_o)$. Therefore, $v_{D2} = V_{\rm in} - v_2 - V_o = (1+\alpha)(V_{\rm in} - V_o) < 0$ and D_2 keeps reverse biased. Meanwhile, $v_{ds\_Q2} = V_{\rm in} - v_2 = (1+\alpha)V_{\rm in} - \alpha V_o$. If $V_{\rm in}/V_o > \alpha/(1+\alpha)$, $v_{ds\_Q2} > 0$ and D_{Q2} remains off. Otherwise, if $V_{\rm in}/V_o < \alpha/(1+\alpha)$, $v_{ds\_Q2} < 0$ and D_{Q2} conducts immediatelly (assuming that the forward-bias voltage of D_{Q2} is 0), which causes a negative direction current flowing through Winding 2, as shown in Fig. 4(b).

Table II summarizes the coupling effects on the circuit statuses of Phase 1 in three different conditions, which are also valid for Phase 2. All these situations, only depending on the relation between the input–output voltage ratio and the coupling coefficient, can be used as the boundaries for the classification of DCM operation modes.

III. OPERATION MODES IN A SWITCHING CYCLE

Theoretically, for the inductor current operating in DCM, the switch duty cycle d can vary from 0 to 1 when $V_{\rm in}/V_o < 0.5$ and vary from 0 to 0.5 when $V_{\rm in}/V_o \ge 0.5$. Therefore, besides the relationship between $V_{\rm in}/V_o$ and α, the duty cycle related with load can also be viewed as a criterion for the classification of the operation modes, such as $d \le 0.5$ and $d > 0.5$. Furthermore, since the coupling effects are remarkable when the two phase currents are overlapped in the time domain, the operation modes can also be characterized by the overlap time of the two winding currents. Therefore, ten DCM operation modes and their main waveforms as shown in Figs. 5 to 8, including switch drive signals, inductor winding voltages and currents, and input current are discussed hereinafter.

1) $d \le 0.5$ and $V_{\rm in}/V_o < \alpha/(1+\alpha)$: There are two operation modes under this condition, as shown in Fig. 5. Before any switch of one phase turns on, the inductor winding current of the other phase has reached 0. The reverse-paralleled diode will conduct in some statuses, and the equivalent inductance will become negative.

For Mode 1a in Fig. 5(a), when Q_1 turns on, i_{L1} increases gradually with the equivalent inductance L_{cp}, and i_{L2} keeps 0. When Q_1 turns off, D_{Q2} conducts as stated in Section II, then $v_1 = V_{\rm in} - V_o$ and $v_2 = V_{\rm in}$. From Table I and Fig. 2, the equivalent inductance of Winding 1 $L_{\rm eq3} > 0$, and the

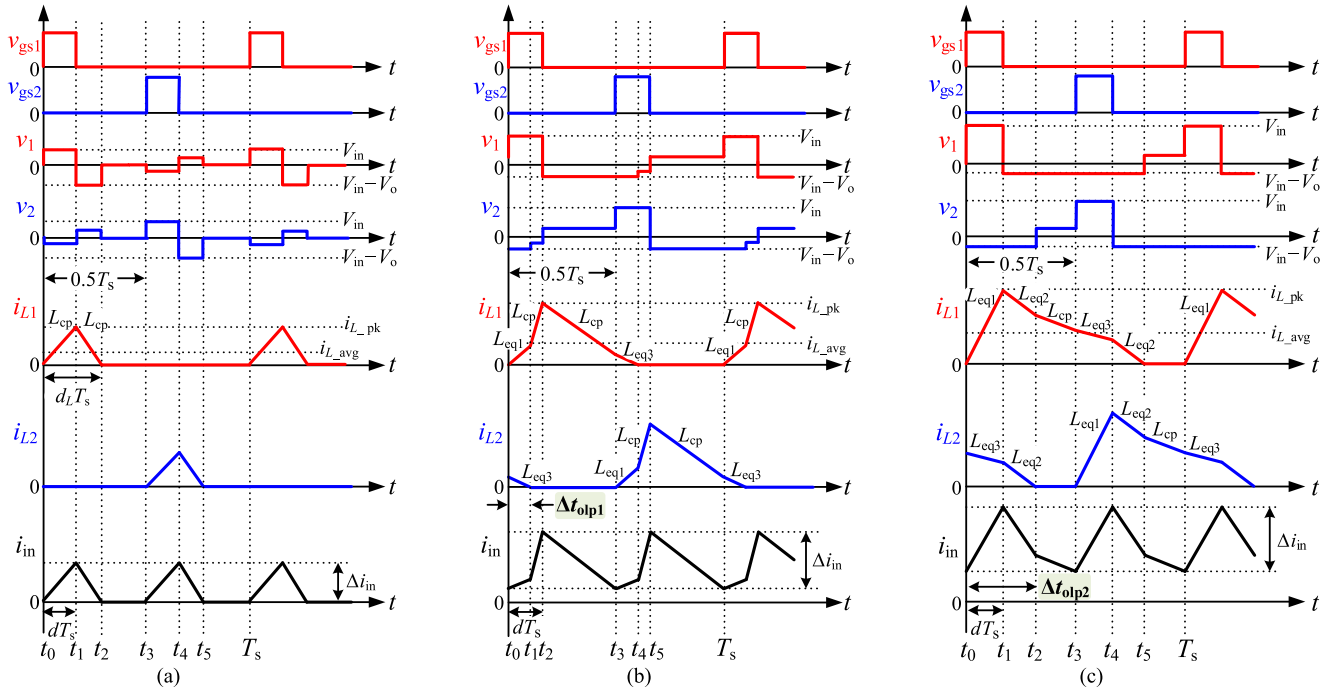

Fig. 6. Waveforms of (a) Mode 2a ($\Delta t_{\rm olp1} < 0$), (b) Mode 2b ($0 < \Delta t_{\rm olp1} \le dT_s$), and (c) Mode 2c ($dT_s < \Delta t_{\rm olp2} < 0.5T_s$) in a switching cycle when $d \le 0.5$ and $\alpha/(1+\alpha) \le V_{\rm in}/V_o \le 1/(1+\alpha)$.

equivalent inductance of Winding 2 $L_{\rm eq1} < 0$. Therefore, i_{L1} starts decreasing while i_{L2} increases from 0 in the negative direction. When i_{L1} reaches 0, D_1 is reverse biased and $v_2 = V_{\rm in}$, $v_1 = -\alpha V_{\rm in}$. Since the equivalent inductance becomes L_{cp}, i_{L2} increases gradually with the slope of $V_{\rm in}/L_{cp}$, and reaches 0 before Q_2 turns on. As a result, current flows through each winding twice with opposite directions in one switching cycle. In Fig. 5(a), $d_{\rm PR}$ is the duty of the duration $[t_1, t_2]$, in which i_{L1} decreases from the peak value to 0. $d_{\rm RR}$ is the duty of the duration $[t_2, t_3]$, in which i_{L2} increases from the negative peak value to 0.

If the duty cycle is increased, i_{L2} cannot reach 0 before the turn-on of Q_2. When Q_2 turns on, i_{L2} flows to 0 and increases in the positive direction continuously. This is defined as Mode 1b and its operation waveforms are provided in Fig. 5(b).

From the waveform of i_{L1} in Fig. 5(a), it can be derived as

$$\begin{cases} \dfrac{V_{\rm in}}{L_{cp}} dT_s = \dfrac{V_o - V_{\rm in}}{L_{\rm eq3}} d_{\rm PR} T_s \\ \dfrac{V_{\rm in}}{-L_{\rm eq1}} d_{\rm PR} T_s = \dfrac{V_{\rm in}}{L_{cp}} d_{\rm RR} T_s \end{cases} \tag{5}$$

and there is a minus before $L_{\rm eq1}$ since $L_{\rm eq1} < 0$. Substituting the equivalent inductance expressions into (5), the $d_{\rm PR}$ and $d_{\rm RR}$ can be expressed as

$$\begin{cases} d_{\rm PR} = \dfrac{\left(1-\alpha^2\right) V_{\rm in}}{V_o - (1+\alpha) V_{\rm in}} d \\ d_{\rm RR} = \dfrac{\alpha V_o - (1+\alpha) V_{\rm in}}{V_o - (1+\alpha) V_{\rm in}} d \end{cases}. \tag{6}$$

The condition of Mode 1a satisfies

$$d + d_{\rm PR} + d_{\rm RR} \le 0.5. \tag{7}$$

Substitution of (6) into (7) yields

$$d \le 1/\left[2\left(1+\alpha\right)\right]. \tag{8}$$

Therefore, the converter operates in Mode 1a when $d \le 1/[2(1+\alpha)]$, and in Mode 1b when $d > 1/[2(1+\alpha)]$.

2) $d \le 0.5$ and $\alpha/(1+\alpha) \le V_{\rm in}/V_o \le 1/(1+\alpha)$: There are three operation modes under this condition, and the wavefroms in a switch cycle are shown in Fig. 6. In this condition, all the equivalent inductances are positive and all the winding currents are in the positive direction.

For Mode 2a in Fig. 6(a), when Q_1 turns on, i_{L1} increases gradually with the equivalent inductance L_{cp}, and i_{L2} keeps 0. When Q_1 turns off, i_{L1} decreases gradually with the slop of $(V_{\rm in} - V_o)/L_{cp}$, and i_{L2} remains 0. As a result, there is no overlap between the two winding currents, and the equivalent inductance is always L_{cp}.

As the input voltage, the load (duty cycle) or L_{cp} is enlarged, the two winding currents will overlap during a time period. If i_{L2} decreases to 0 within the conduction period of Q_1, i.e., the overlap time of i_{L1} and i_{L2} $\Delta t_{\rm olp1} \le dT_s$, i_{L1} will increase with $L_{\rm eq1}$ and i_{L2} will decrease with $L_{\rm eq3}$, respectively. This is defined as Mode 2b, as shown in Fig. 6(b). If i_{L2} does not decreases to 0 after Q_1 turns off, i.e., the currents overlap time $\Delta t_{\rm olp2} > dT_s$, initially, i_{L1} will increase with $L_{\rm eq1}$ and i_{L2} will decrease $L_{\rm eq3}$, and then both winding currents will decrease with $L_{\rm eq2}$ after the time point at which Q_1 turns off. This is defined as Mode 2c, as shown in Fig. 6(c).

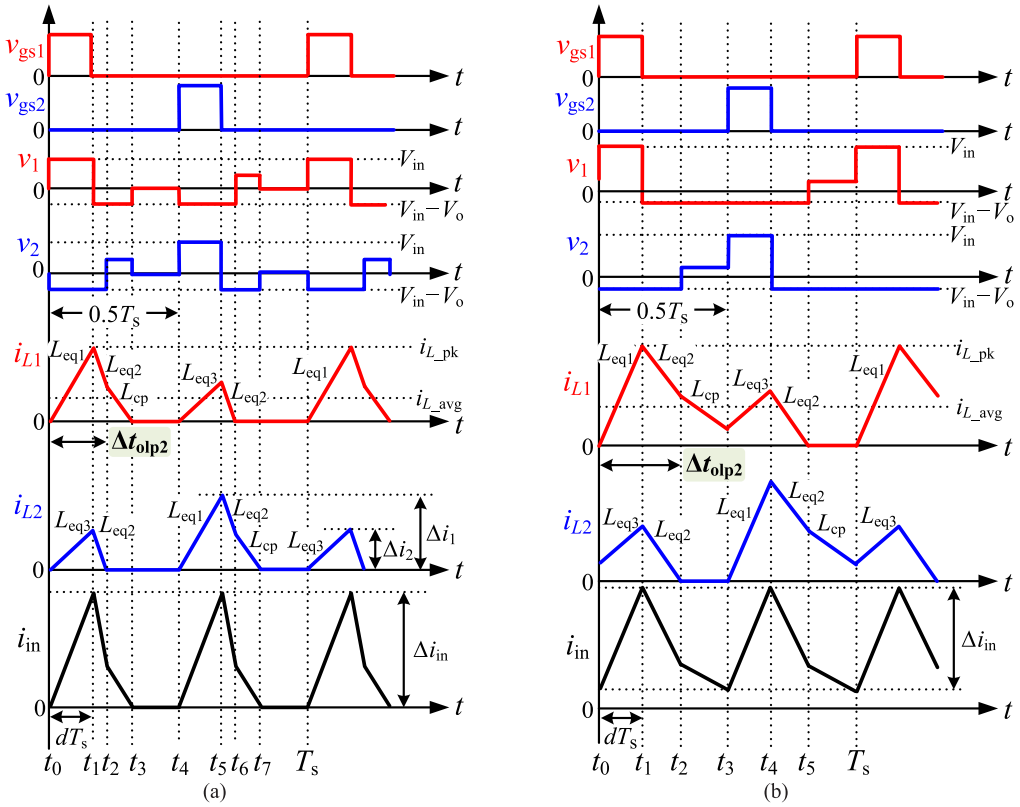

Fig. 7. Waveforms of (a) Mode 3a and (b) Mode 3b in a switching cycle when $d \leq 0.5$ and $V_{\text{in}}/V_o > 1/(1+\alpha)$.

For Mode 2a, take the voltage balance into consideration, the duty cycle satisfies

$$d \leq (V_o - V_{\text{in}})/(2V_o). \tag{9}$$

From the inductor winding current of Mode 2b in Fig. 6(b), it can be obtained that

$$\frac{V_{\text{in}} \cdot \Delta t_{\text{olp1}}}{L_{\text{eq1}}} + \frac{V_{\text{in}}}{L_{cp}}\left(dT_s - \Delta t_{\text{olp1}}\right) = \frac{V_o - V_{\text{in}}}{L_{cp}}\left(\frac{1}{2} - d\right)T_s + \frac{V_o - V_{\text{in}}}{L_{\text{eq3}}}\Delta t_{\text{olp1}}, \tag{10}$$

and Δt_{olp1} can be derived as

$$\Delta t_{\text{olp1}} = \frac{(1-\alpha)\left[V_{\text{in}} - (1-2d)\,V_o\right]}{2\left[V_o - (1+\alpha)\,V_{\text{in}}\right]} \cdot T_s. \tag{11}$$

If $0 < \Delta t_{\text{olp1}} \leq dT_s$, the duty cycle will satisfy

$$\frac{V_o - V_{\text{in}}}{2V_o} < d \leq \max\left\{\frac{(1-\alpha)\,(V_o - V_{\text{in}})}{2\left[V_{\text{in}}\,(1+\alpha) - V_o\alpha\right]},\ 0.5\right\}. \tag{12}$$

For Mode 2c, an equation, from the waveform of i_{L1} in Fig. 6(c), can be obtained as

$$\frac{V_{\text{in}}}{L_{\text{eq1}}}dT_s = \frac{V_o - V_{\text{in}}}{L_{\text{eq3}}}dT_s + 2\frac{V_o - V_{\text{in}}}{L_{\text{eq2}}}\left(\Delta t_{\text{olp2}} - dT_s\right) + \frac{V_o - V_{\text{in}}}{L_{\text{cp}}}\left(\frac{T_s}{2} - \Delta t_{\text{olp2}}\right) \tag{13}$$

and Δt_{olp2} can be derived as

$$\Delta t_{\text{olp2}} = \frac{(1-\alpha)\,V_{\text{in}} - (1-\alpha-2d)\,V_o}{2\,(V_o - V_{\text{in}})\,(1+\alpha)} \cdot T_s. \tag{14}$$

If $dT_s < \Delta t_{\text{olp2}} < 0.5T_s$, the duty cycle will satisfy

$$\max\left\{\frac{(1-\alpha)\,(V_o - V_{\text{in}})}{2\left[V_{\text{in}}\,(1+\alpha) - V_o\alpha\right]},\ \frac{V_o - V_{\text{in}}}{2V_o}\right\} < d < \frac{V_o - V_{\text{in}}}{V_o}. \tag{15}$$

3) $d \leq 0.5$ and $V_{\text{in}}/V_o > 1/(1+\alpha)$: There are two operation modes under this condition, as shown in Fig. 7. The power diode will conduct under force in some statuses, and the equivalent inductance will become negative.

For Mode 3a, as shown in Fig. 7(a), when Q_1 turns on, D_2 is forward biased, and $v_1 = V_{\text{in}}$, $v_2 = V_{\text{in}} - V_o$. From Table I and Fig. 2, the equivalent inductance of Winding 1 $L_{\text{eq1}} > 0$ and the equivalent inductance of Winding 2 $L_{\text{eq3}} < 0$. Therefore, i_{L1} and i_{L2} both increase from 0 in the positive direction. When Q_1 turns off, $v_1 = v_2 = V_{\text{in}} - V_o$, and i_{L1} and i_{L2} decrease together with the slope of $(V_{\text{in}} - V_o)/L_{\text{eq2}}$. Since the value of i_{L2} at t_1 is normally lower than that of i_{L1}, i_{L2} reaches 0 earlier, and i_{L1} reaches 0 before the turn-on of Q_2. As a result, current flows through each winding in the positive direction twice in one switching cycle.

If the inductor current cannot reach 0 within the initial half switching period due to the enlarged duty cycle or L_{cp}, the two DCM currents will join together as only one continuous current flow in one switching cycle, and the two winding currents

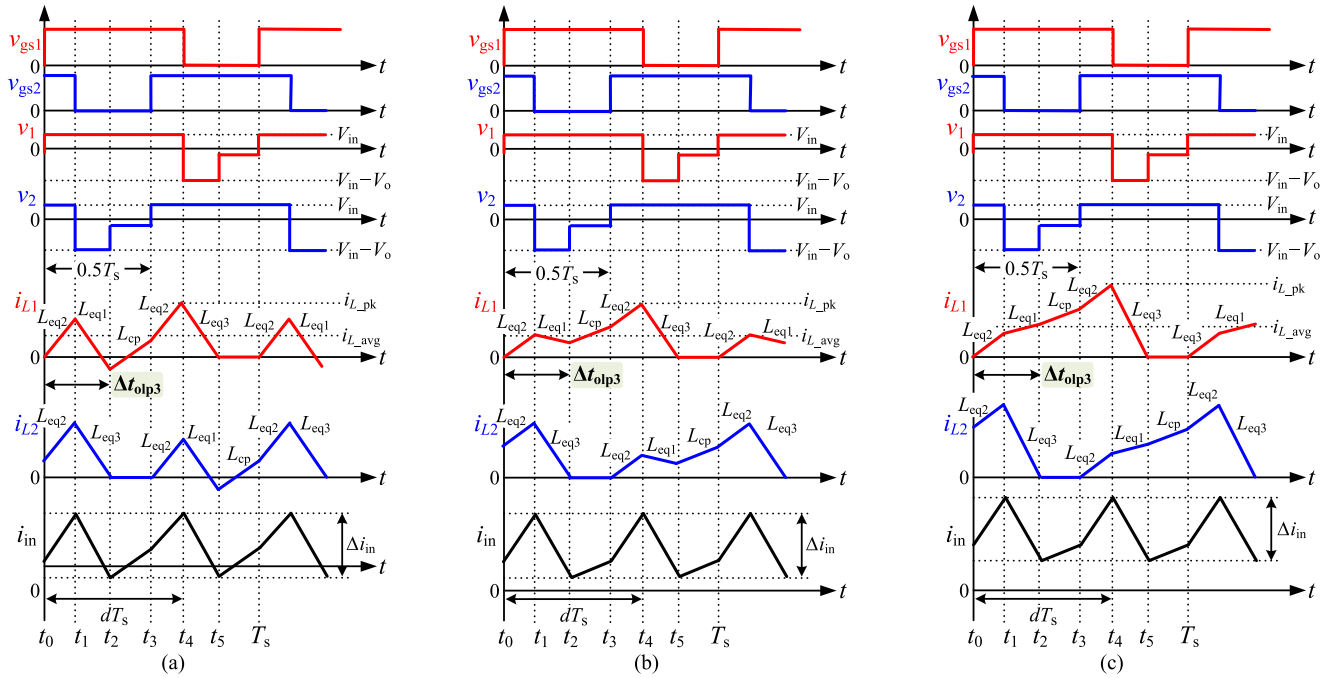

Fig. 8. Waveforms of (a) Mode 4a $[V_{\rm in}/V_o < \alpha/(1+\alpha)]$, (b) Mode 4b $[V_{\rm in}/V_o < \alpha/(1+\alpha)]$, and (c) Mode 5 $[\alpha/(1+\alpha) \le V_{\rm in}/V_o \le 0.5]$ in a switching cycle for $d > 0.5$.

TABLE III
DISTRIBUTION OF OPERATION MODES

	$V_{\rm in}/V_o < \alpha/(1+\alpha)$	$\alpha/(1+\alpha) \le V_{\rm in}/V_o \le 1/(1+\alpha)$	$V_{\rm in}/V_o > 1/(1+\alpha)$
$d \le 0.5$	Mode 1a, Mode1b	Mode 2a, Mode 2b, Mode 2c	Mode 3a, Mode 3b
$d > 0.5$	Mode 4a, Mode 4b	Mode 5 $(\alpha/(1+\alpha) \le V_{\rm in}/V_o \le 0.5)$	

overlap during a period of time $\Delta t_{\rm olp2}$. This is defined as Mode 3b, as shown in Fig. 7(b). For Mode 3b, the duty cycle of i_{L1} in the first half switching period is less than 0.5, and the duty cycle also complies with a voltage balance. Therefore, the duty cycle also satisfies $d \le (V_o - V_{\rm in})/(2V_o)$. For Mode 3b, its waveforms are similar to that of Mode 2c, and its duty cycle also obeys (15).

4) $d > 0.5$: For $d > 0.5$, if $V_{\rm in}/V_o > 0.5$, the inductor current will not reach 0 at the end of one switching cycle and the current will be continuous. Hence, this paper only discusses the case of $V_{\rm in}/V_o \le 0.5$. Generally, there are three operation modes, as shown in Fig. 8.

For $V_{\rm in}/V_o < \alpha/(1+\alpha)$, when Q_1 turns on, Q_2 remains on. The two winding currents increase with the slope of $V_{\rm in}/L_{\rm eq2}$ simultaneously. When Q_2 turns off, $v_1 = V_{\rm in}$, $v_2 = V_{\rm in} - V_o$, and i_{L1} and i_{L2} decrease together since their equivalent inductances $L_{\rm eq1} < 0$ and $L_{\rm eq3} > 0$. When i_{L2} reaches 0, $v_1 = V_{\rm in}$, $v_2 = -\alpha V_{\rm in}$, and i_{L1} increases with the slope of $V_{\rm in}/L_{cp}$ until the conduction of Q_2. In the second half switching cycle, the current waveform of i_{L1} is as the same as the waveform of i_{L2} in the first half switching cycle. The two winding currents overlap during a period of time $\Delta t_{\rm olp3}$. When Q_1 conducts and Q_2 remains OFF, if i_{L1} decreases faster and reaches 0 earlier than i_{L2}, the current will continuously increase in the negative direction until i_{L2} reaches 0. This is defined as Mode 4a, as shown in Fig. 8(a). If i_{L1} does not decrease to 0 before i_{L2} reaches 0, Mode 4b will occur, as shown in Fig. 8(b).

For $\alpha/(1+\alpha) \le V_{\rm in}/V_o \le 0.5$, the current waveforms are similar to that of Mode 4b. The only difference lies in the period $[t_1, t_2]$ for i_{L1} and $[t_4, t_5]$ for i_{L2}, during both of which the equivalent inductance $L_{\rm eq1}$ alters from negative to positive, and the current slope becomes positive. This is defined as Mode 5, as shown in Fig. 8(c).

For $d > 0.5$, i_{L1} rises from 0 and falls back to 0 in one switching cycle, so it obeys

$$\frac{V_{\rm in}(2d-1)T_s}{L_{\rm eq2}} + \frac{V_{\rm in}(0.5T_s - \Delta t_{\rm olp3})}{L_{cp}} = \frac{V_o - V_{\rm in}}{L_{\rm eq3}}[\Delta t_{\rm olp3} - (d-0.5)T_s] + \frac{V_{\rm in}[\Delta t_{\rm olp3} - (d-0.5)T_s]}{-L_{\rm eq1}} \quad (16)$$

where $L_{\rm eq1} < 0$. So, $\Delta t_{\rm olp3}$ can be derived as

$$\Delta t_{\rm olp3} = \frac{(2d-1)V_o + (1-\alpha)V_{\rm in}}{2[V_o - (1+\alpha)V_{\rm in}]} \cdot T_s. \quad (17)$$

For Mode 4a, it satisfies

$$\frac{V_{\rm in}(d-0.5)T_s}{L_{\rm eq2}} < \frac{V_{\rm in}[\Delta t_{\rm olp3} - (d-0.5)T_s]}{-L_{\rm eq1}}. \quad (18)$$

Substituting (17) into (18) yields

$$d < 1 - \frac{V_{\rm in}}{2V_o} - \frac{1}{2(1+\alpha)}. \quad (19)$$

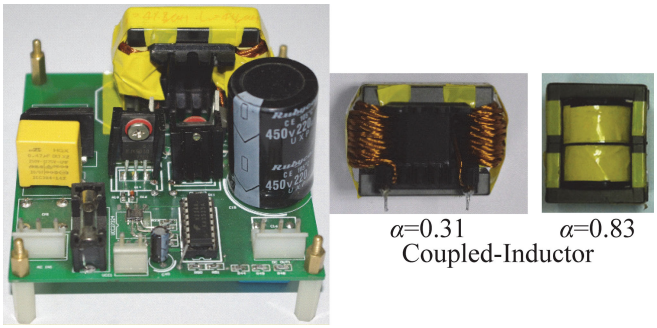

Fig. 9. Experimental prototype and coupled inductor under test.

Therefore, for $V_{\rm in}/V_o < \alpha/(1+\alpha)$, Mode 4a occurs when $0.5 < d < 1-(V_{\rm in}/2V_o)-[1/2(1+\alpha)]$, and Mode 4b occurs when $1-(V_{\rm in}/2V_o)-[1/2(1+\alpha)] \le d \le 1-(V_{\rm in}/V_o)$. For $\alpha/(1+\alpha) \le V_{\rm in}/V_o \le 0.5$, Mode 5 occurs when $d > 0.5$.

Table III shows the mode distribution based on the relation between α and $V_{\rm in}/V_o$.

IV. Experimental Verification

A 300-W two-phase interleaved boost dc–dc converter and two coupled inductors with different coupling coefficients are fabricated for the experimental verification, as shown in Fig. 9. $V_o = 390\,\text{Vdc}$; $P_{o\_\text{rated}} = 300\,\text{W}$; $f_s = 100\,\text{kHz}$. One coupled inductor has a relatively low coupling-coefficient of $\alpha = 0.31$ with $L_{cp} = 41.8\,\mu\text{H}$, (ferrite core: EI40/35, air gaps of the center and outer legs: $\delta = 2.60$ mm, turns number for each phase: 28), and the other one has a high coupling-coefficient of $\alpha = 0.83$ with $L_{cp} = 100\,\mu\text{H}$ (ferrite core: EER28/34, air gaps of the center and outer legs: $\delta = 0.6$ mm, turns number for each phase: 32). All the experimental waveforms are tested under a relative light-load condition to make sure that the converter is operating in DCM, and both the input voltage and duty cycle are varied to verify the validity of the analysis above.

1) $d \le 0.5$ and $V_{\rm in}/V_o < \alpha/(1+\alpha)$: For $V_o = 390\,\text{V}$ and $\alpha = 0.31$, the boundary input voltage is $\alpha V_o/(1+\alpha) = 92\,\text{V}$ and the boundary duty cycle of the operation mode is $1/2(1+\alpha) = 0.38$. When $d < 0.38$, the converter operates in Mode 1a, as shown in Fig. 10(a). When Q_1 turns off, both winding currents decrease positively and negatively, simultaneously. i_{L2} decreases until i_{L1} reaches 0, and then increases to 0 without a turn-on switch drive signal which means that D_{Q2} conducts. The ringing current between the intervals of currents in the opposite direction is caused by the resonation of parasitic parameters and the reverse-recovery current of the reverse-paralleled diode [9]. When $d > 0.38$, the converter will operate at Mode 1b, as shown in Fig. 10(b). The two opposite currents in one winding become continuous, which matches the theoretical analysis above.

For $V_o = 390\,\text{V}$ and $\alpha = 0.83$, $\alpha V_o/(1+\alpha) = 177$ V and $1/2(1+\alpha) = 0.27$. Fig. 10(c) shows the operation waveforms in the duty cycle boundary condition, of which the opposite currents just join together at the time when the switch turns on, as shown in the dashed circle. For a condition with a larger duty cycle shown in Fig. 10(d), although the switch conducts and a negative current flow through its winding, the current waveform

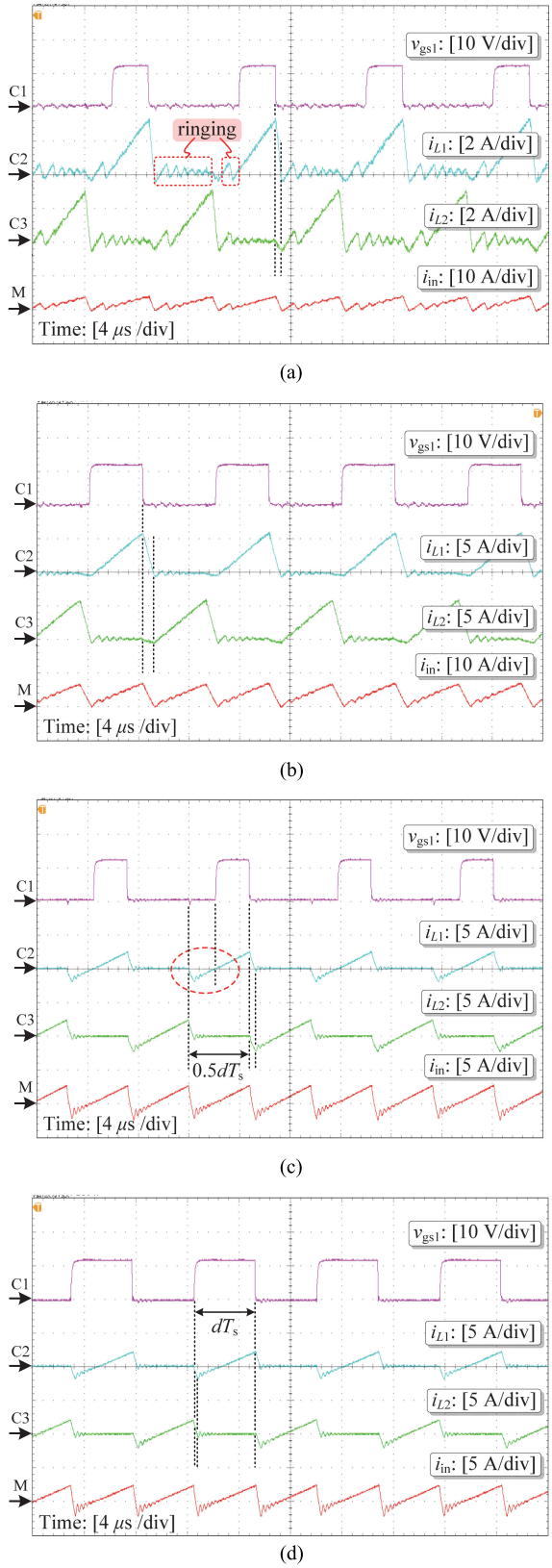

Fig. 10. Typical experimental waveforms of v_{gs1}, i_{L1}, i_{L2}, and $i_{\rm in}$ when $d \le 0.5$ and $V_{\rm in} < \alpha V_o/(1+\alpha)$, including (a) Mode 1a ($\alpha = 0.31$, $L_{cp} = 41.8\,\mu\text{H}$, $V_{\rm in} = 48\,\text{V}$, $d = 0.28 < 0.38$), (b) Mode 1b ($\alpha = 0.31$, $L_{cp} = 41.8\,\mu\text{H}$, $V_{\rm in} = 75\,\text{V}$, $d = 0.41 > 0.38$), (c) Mode 1b ($\alpha = 0.83$, $L_{cp} = 100\,\mu\text{H}$, $V_{\rm in} = 125\,\text{V}$, $d = 0.27$), and (d) Mode 1b ($\alpha = 0.83$, $L_{cp} = 100\,\mu\text{H}$, $V_{\rm in} = 116\,\text{V}$, $d = 0.49 > 0.27$).

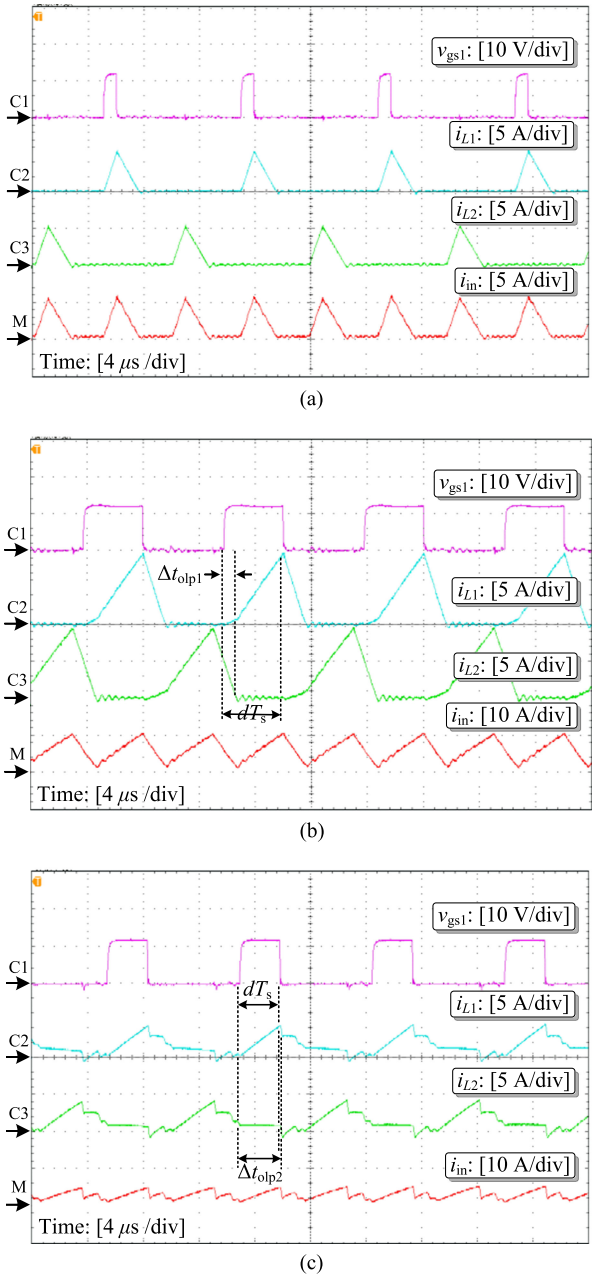

Fig. 11. Typical experimental waveforms of v_{gs1}, i_{L1}, i_{L2}, and $i_{\rm in}$ when d≤0.5 and $\alpha V_o/(1+\alpha) < V_{\rm in} < V_o/(1+\alpha)$, including (a) Mode 2a ($\alpha = 0.31$, $L_{cp} = 41.8\,\mu$H, $V_{\rm in} = 251\,$V, $d = 0.08 < 0.18$), (b) Mode 2b ($\alpha = 0.31$, $L_{cp} = 41.8\,\mu$H, $V_{\rm in} = 121\,$V, $d = 0.41 > 0.34$), and (c) Mode 2c ($\alpha = 0.83$, $L_{cp} = 100\,\mu$H, $V_{\rm in} = 207\,$V, $d = 0.297 > 0.28$).

still depends on the winding current of the other phase, which suggests the coupling effects.

2) $d \le 0.5$ and $\alpha/(1+\alpha) \le V_{\rm in}/V_o \le 1/(1+\alpha)$: For $V_o = 390\,$V and $\alpha = 0.31$, $\alpha V_o/(1+\alpha) = 92\,$V and $V_o/(1+\alpha) = 297\,$V. When $V_{\rm in} = 251\,$V and $d = 0.08$ (the boundary duty cycle for $V_{\rm in} = 251\,$V is (390−251)/(2 × 390) = 0.18), the converter operates in Mode 2a as shown in Fig. 11(a), and the mode is just like the discrete inductor case. This mode is more common in high-input voltage cases due to the very small duty cycle. When $V_{\rm in} = 121\,$V and $d =$

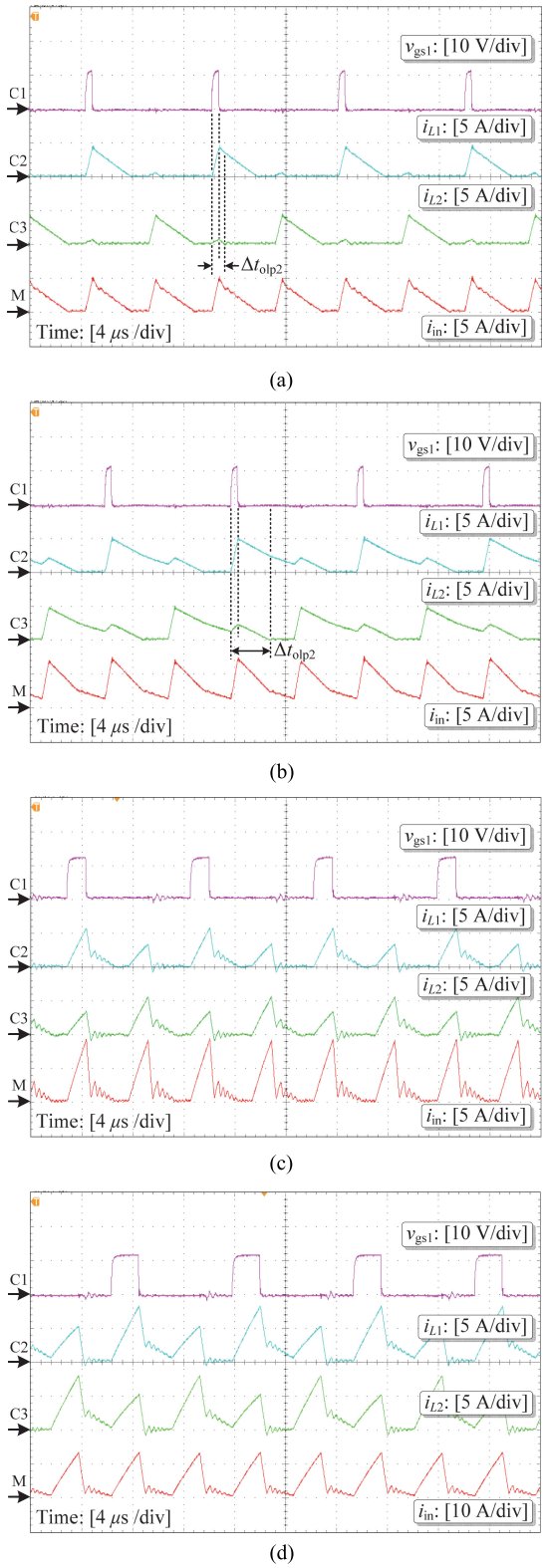

Fig. 12. Typical experimental waveforms of $v_{\rm gs1}$, $i_{\rm L1}$, $i_{\rm L2}$, and $i_{\rm in}$ when d≤0.5 and $V_{\rm in} > V_o/(1+\alpha)$, including (a) Mode 3a ($\alpha = 0.31$, $L_{cp} = 41.8\,\mu$H, $V_{\rm in} = 327\,$V, $d = 0.045 < 0.08$), (b) Mode 3b ($\alpha = 0.31$, $L_{cp} = 41.8\,\mu$H, $V_{\rm in} = 367\,$V, $d = 0.045 > 0.029$), (c) Mode 3a ($\alpha = 0.83$, $L_{cp} = 100\,\mu$H, $V_{\rm in} = 240\,$V, $d = 0.15 < 0.19$), and (d) Mode 3b ($\alpha = 0.83$, $L_{cp} = 100\,\mu$H, $V_{\rm in} = 240\,$V, $d = 0.22 > 0.19$).

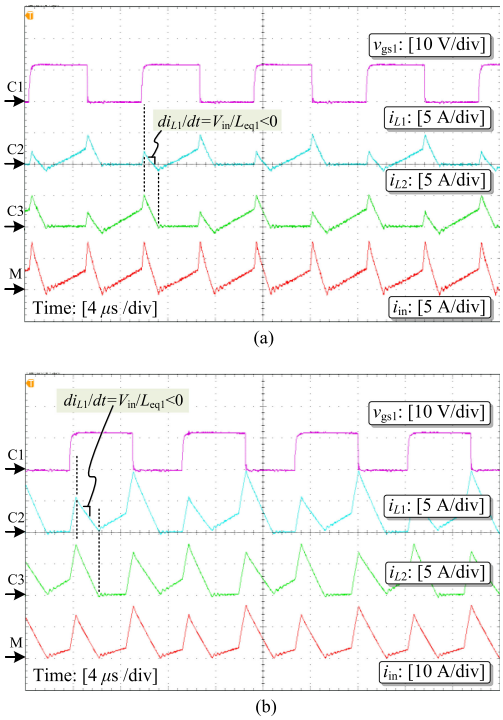

Fig. 13. Typical experimental waveforms of v_{gs1}, i_{L1}, i_{L2} and $i_{\rm in}$ when d>0.5 and $V_{\rm in} < \alpha V_o/(1+\alpha)$, including (a) Mode 4a ($\alpha = 0.83$, $L_{cp} = 100\,\mu$H, $V_{\rm in} = 148\,$V, $d = 0.51$), and (b) Mode 4b ($\alpha = 0.83$, $L_{cp} = 100\,\mu$H, $V_{\rm in} = 148\,$V, $d = 0.55$).

0.41, the boundary duty cycle is (390−121)/(2 × 390) = 0.34, and the converter operates in Mode 2b as shown in Fig. 11(b), where the currents of two windings overlap and $\Delta t_{\rm olp1} \le dT_s$.

For $V_o = 390\,$V and $\alpha = 0.83$, $\alpha V_o/(1+\alpha) = 177\,$V and $V_o/(1+\alpha) = 213\,$V. When $V_{\rm in} = 207\,$V and $d = 0.297$ (the boundary duty cycle is $\frac{(1-0.83)(390-207)}{2[207(1+0.83)-390\times 0.83]} = 0.28$), $\Delta t_{\rm olp2} > dT_s$ and the converter operates in Mode 2c, as shown in Fig. 11(c).

3) $d \le 0.5$ and $V_{\rm in}/V_o > 1/(1+\alpha)$: In this condition, when the switch of any phase turns on, current flows through both windings with a positive slope, regardless of whether the initial current is 0 or not. For $\alpha = 0.31$ and a fixed working duty cycle $d = 0.045$, when $V_{\rm in} = 327\,$V, the boundary duty cycle is $(V_o - V_{\rm in})/(2V_o) = (390-327)/(2\times 390) = 0.08$, so the converter operates in Mode 3a, as shown in Fig. 12(a), and when $V_{\rm in} = 367\,$V, the boundary duty cycle is $(V_o - V_{\rm in})/(2V_o) = (390-367)/(2\times 390) = 0.029$, and the converter operates in Mode 3b, as shown in Fig. 12(b). For $\alpha = 0.83$ and $V_{\rm in} = 240\,$V ($V_{\rm in} > 213\,$V), the boundary duty cycle is (390−240)/(2 × 390) = 0.19, so the change of the duty cycle also causes the operation mode transformation, as shown in Fig. 12(c) and (d).

4) $d > 0.5$: This condition more likely occurs when L_{cp} is large or the coupling coefficient is high, and the two winding currents keep overlapped. For $\alpha = 0.83$ and $V_{\rm in} = 148\,$V ($V_{\rm in} < 177\,$V), the boundary duty cycle $d = 0.53$ (calculated from (19)). The Mode 4a and Mode 4b waveforms are shown in Fig. 13(a) and (b) under different duty cycles of $d = 0.51$ and $d = 0.55$, respectively. As seen, the two winding currents increase together when both switches are on and decrease when any switch turns off. The winding current may flow in the negative direction under a light-load condition (smaller duty cycle), as shown in Fig. 13(a).

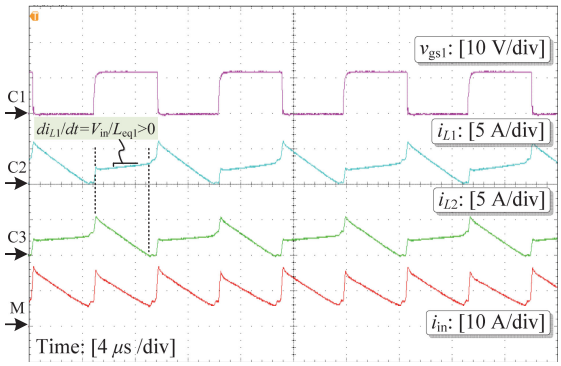

Fig. 14. Typical experimental waveforms of v_{gs1}, i_{L1}, i_{L2}, and $i_{\rm in}$ when $d > 0.5$ and $\alpha V_o/(1+\alpha) \le V_{\rm in} \le 0.5V_o$, which is in Mode 5 ($\alpha = 0.83$, $L_{cp} = 100\,\mu$H, $V_{\rm in} = 189\,$V, $d = 0.51$).

When $V_{\rm in} = 189\,$V ($177\,$V $< V_{\rm in} <$ $195\,$V $(V_o/2)$) and $d = 0.51$, Mode 5 is shown in Fig. 14. The winding current is positive. The main difference between Mode 4 and Mode 5 is the current slope in one phase during which a switch turns off and the other one remains on, which represents the sign change of the equivalent inductance caused by coupling effects.

V. Conclusion

The two-phase interleaved boost dc–dc converter with coupled inductors is analyzed in detail based on the fundamental circuit statuses. From the analysis of equivalent inductances of DCM operation modes, it is found out that under specific conditions determined by the relations between the input–output voltage ratio and the coupling coefficient, the sign of the equivalent inductance is changed and the power diode or reverse-paralleled diode will conducts under force. This coupling effects on the circuit statuses are independent of the converter load (duty cycle), and their condition boundaries can be used to classify the DCM operation modes. As a result, three major operation regions are introduced, and ten DCM operation modes as well as their key waveforms and boundary conditions under varied input–output voltage ratios and loads (duty cycles) are analyzed comprehensively. Since the classification was based on the physical parameters of the converter and its operation conditions, the operation mode under a given condition can be predicted easily. The analysis can also be extended directly to the interleaved buck converter with coupled inductors in DCM.

References

[1] W. Martinez, S. Kimura, J. Imaoka, and M. Yamamoto, "Volume comparison of DC-DC converters for electric vehicles," in *Proc. IEEE Workshop Power Electron. Power Qual. Appl.*, 2015, pp. 1–6.

[2] M. Hirakawa, M. Nagano, Y. Watanabe, K. Andoh, S. Nakatomi, and S. Hashino, "High power density DC/DC converter using the close-coupled-inductors," in *Proc. IEEE Energy Convers. Congr. Expo.*, 2009, pp. 1760–1767.

[3] S. Kimura, Y. Itoh, W. Martine, M. Yamamoto, and J. Imaoka, "Downsizing effects of integrated magnetic components in high power density DC–DC converters for EV and HEV applications," *IEEE Trans. Ind. Appl.*, vol. 52, no. 4, pp. 2693–2704, Dec. 2014.

[4] M. Pavlovsk´y, G. Guidi, and A. Kawamura, "Assessment of coupled and independent phase designs of interleaved multiphase buck/boost DC–DC converter for EV power train," *IEEE Trans. Power Electron.*, vol. 29, no. 6, pp. 2693–2704, Dec. 2014.
[5] S. Chandrasekaran and L. U. Gokdere, "Integrated magnetics for interleaved dc-dc boost converter for fuel cell powered vehicles," in *Proc. IEEE Power Electron. Spec. Conf.*, 2004, pp. 356–361.
[6] K. J. Hartnett, J. G. Hayes, M. S. Ryłko, B. J. Barry, and J. W. Masłon, "Comparison of 8-kW CCTT IM and discrete inductor interleaved boost converter for renewable energy applications," *IEEE Trans. Ind. Appl.*, vol. 51, no. 3, pp. 2455–2469, May/Jun. 2015.
[7] J. Imaoka, Y. Ishikura, T. Kawashima, and M. Yamamoto, "Optimal design method for interleaved single-phase PFC converter with coupled-inductor," in *Proc. IEEE Energy Convers. Congr. Expo.*, 2011, pp. 1807–1812.
[8] F. Yang, X. Ruan, Y. Yang, and Z. Ye, "Interleaved critical current mode boost PFC converter with coupled-inductor," *IEEE Trans. Power Electron.*, vol. 26, no. 9, pp. 2404–2413, Sep. 2011.
[9] J. W. Kolar, G. R. Kamath, N. Mohan, and F. C. Zach, "Self-adjusting input current ripple cancellation of coupled parallel connected hysteresis-controlled boost power factor correctors," in *Proc. IEEE Power Electron. Spec. Conf.*, 1998, pp. 164–173.
[10] E. Labouré, A. Cunière, T. A. Meynard, F. Forest, and E. Sarraute, "A theoretical approach to intercell transformers, application to interleaved converters," *IEEE Trans. Power Electron.*, vol. 23, no. 1, pp. 464–473, Jan. 2008.
[11] H. Kosai, S. Mcneal, B. Jordan, J. Scofield, B. Ray, and Z. Turgut, "Coupled inductor characterization for a high performance interleaved boost converter," *IEEE Trans. Magn.*, vol. 45, no. 10, pp. 4812–4815, Oct. 2009.
[12] D. O. Boillat and J. W. Kolar, "Modeling and experimental analysis of a coupling Inductor employed in a high performance AC power source," in *Proc. Int. Conf. Renewable Energy Res. Appl.*, 2012, pp. 1–18.
[13] X. Huang, X. Wang, T. Nergaard, J. Lai, X. Xu, and L. Zhu, "Parasitic ringing and design issues of digitally controlled high power interleaved boost converters," *IEEE Trans. Power Electron.*, vol. 19, no. 5, pp. 1341–1352, Sep. 2004.
[14] B Ray, H Kosai, S Mcneal, B Jordan, and J Scofield, "A comprehensive multi-mode performance analysis of interleaved boost converters," in *Proc. IEEE Energy Convers. Congr. Expo.*, 2010, pp. 3014–3021.
[15] B. C. Barry, J. G. Hayes, and M. S. Ryłko, "CCM and DCM operation of the interleaved two-phase boost converter with discrete and coupled-inductors," *IEEE Trans. Power Electron.*, vol. 30, no. 12, pp. 6551–6567, Dec. 2015.
[16] D. Wu, G. Calderon-Lopez, and A. J. Forsyth, "Discontinuous conduction/current mode analysis of dual interleaved buck and boost converters with interphase transformer," *IET Power Electron.*, vol. 9, no. 1, pp. 31–41, Jan. 2015.
[17] J. Li, C. R. Sullivan, and A. Schultz, "Coupled inductor design optimization for fast-response low-voltage dc-dc converters," in *Proc. IEEE Appl. Power Electron. Conf.*, 2002, pp. 817–823.
[18] P. Zumel, O. Farcia, J. A. Cobos, and J. Uceda, "Tight magnetic coupling in multiphase interleaved converter based on simple transformers," in *Proc. IEEE Appl. Power Electron. Conf.*, 2005, pp. 385–391.
[19] G. Zhu, B. A. McDonald, and K. Wang, "Modeling and analysis of coupled inductors in power converters," *IEEE Trans. Power Electron.*, vol. 26, no. 5, pp. 1355–1363, May 2011.
[20] P. L. Wong, P. Xu, P. Yang, and F. C. Lee, "Performance improvements of interleaving VRMs with coupling inductors," *IEEE Trans. Power Electron.*, vol. 16, no. 4, pp. 499–507, Jul. 2001.

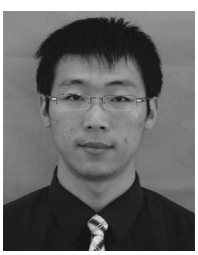

Fei Yang (M'16) was born in Shanxi, China, in 1983. He received the B.S. and Ph.D. degrees in electrical engineering from Nanjing University of Aeronautics and Astronautics, Nanjing, China, in 2006 and 2013, respectively.

In 2015, he joined the Faculty of Electrical Engineering Teaching and Research Division, School of Automation, Nanjing University of Science and Technology, and has been involved in teaching and research in the field of power electronics. From February 2014 to October 2015, he was a Postdoctoral Research Fellow in the Department of Mechanical Engineering, KU Leuven, Leuven, Belgium. His main research interests include PFC converters, EMI filter design, and pulse power generator for electrical discharge machine.

Xinbo Ruan (M'97–SM'02–F'16) was born in Hubei Province, China, in 1970. He received the B.S. and Ph.D. degrees in electrical engineering from Nanjing University of Aeronautics and Astronautics (NUAA), Nanjing, China, in 1991 and 1996, respectively.

In 1996, he joined the Faculty of Electrical Engineering, Teaching and Research Division, NUAA, where he became a Professor with the College of Automation Engineering in 2002 and has been involved in teaching and research in the field of power electronics. From August to October 2007, he was a Research Fellow in the Department of Electronic and Information Engineering, Hong Kong Polytechnic University, Hong Kong, China. From 2008 to 2011, he was also with the College of Electrical and Electronic Engineering, Huazhong University of Science and Technology, China. He is a Guest Professor with Beijing Jiaotong University, Beijing, China,with Hefei University of Technology, Hefei, China, and with Wuhan University, Wuhan, China. He is the author or coauthor of eight books and more than 200 technical papers published in journals and conferences. His main research interests include soft-switching dc–dc converters, soft-switching inverters, power factor correction converters, modeling the converters, power electronics system integration, and renewable energy generation system.

Dr. Ruan received the Delta Scholarship by the Delta Environment and Education Fund in 2003 and was appointed as the Special Appointed Professor of the Chang Jiang Scholars Program by the Ministry of Education, China, in 2007. From 2005 to 2013, he had been serving as the Vice President of the China Power Supply Society, and from 2014 to 2016, he had been serving as the Vice Chair of the Technical Committee on Renewable Energy Systems within the IEEE Industrial Electronics Society. He is currently an Associate Editor for the IEEE TRANSACTIONS ON INDUSTRIAL ELECTRONICS, the IEEE TRANSACTIONS ON POWER ELECTRONICS, the IEEE JOURNAL OF EMERGING AND SELECTED TOPICS ON POWER ELECTRONICS, and the IEEE TRANSACTIONS ON CIRCUITS AND SYSTEMS—PART II.

Gang Wu (S'12) was born in Jiangsu Province, China, in 1989. He received the B.S. degrees in electrical engineering and automation from Nanjing University of Aeronautics and Astronautics, Nanjing, China, in 2011, where he is currently working toward the Ph.D. degree in electrical engineering.

His current research interests include high step-up dc–dc converter and renewable energy generation systems.

Zhihong Ye (M'00) was born in Zhejiang Province, China, in 1969. He received the B.S. and M.S. degrees in electrical engineering from Tsinghua University, Beijing, China, in 1992 and 1994, respectively, and the Ph.D. degree from the Bradley Department of Electrical and Computing Engineering, Virginia Polytechnic Institute and State University, Blacksburg, VA, USA, in 2000.From 2000 to 2005, he was with General Electric Global Research Center as an Electrical Engineer in Niskayuna, NY, USA. From 2005 to 2006, he was with Dell as a Commodity Quality Manager. Since 2006, he has been with LiteOn Technology, Corp., Nanjing, China, as the Director of Research and Development. He holds 17 U.S. patents, and has published more than 30 technical papers in transactions and international conferences. His research interests include high density, high-efficiency power supply for computing, communication, and consumer electronics applications, digital control, power converter topologies and controls, soft-switching techniques, etc.